

Design of magnetoelectric coupling in ferroelectric metal

Wang Zhang(张旺) and Xue-Zeng Lu(逯学曾)

Citation: Chin. Phys. B, 2026, 35 (**7**): 077506. DOI: 10.1088/1674-1056/ae6173
http://cpb.iphy.ac.cn; http://iopscience.iop.org/cpb

What follows is a list of articles you may be interested in

The rise of van der Waals multiferroic heterostructures: Interfacial physics and devices

Yihao Zhao(赵一豪), Hongxu Duan(段虹旭), Tai Min(闵泰), and Tao Li(李桃)
Chin. Phys. B, 2026, 35 (**6**): 067501. DOI: 10.1088/1674-1056/ae3e73

Magnetoelectric topology: The rope weaving in parameter space

Ying Zhou(周颖), Ziwen Wang(王子文), Fan Wang(王凡), Haoshen Ye(叶浩燊), and Shuai Dong(董帅)
Chin. Phys. B, 2026, 35 (**2**): 027501. DOI: 10.1088/1674-1056/ae2c6b

Distance-dependent magnetization modulation induced by inter-superatomic interactions in Cr-doped $Au_6Te_{12}Se_8$ dimers

Yurou Guan(官雨柔), Nanshu Liu(刘南舒), Cong Wang(王聪), Fei Pang(庞斐), Zhihai Cheng(程志海), and Wei Ji(季威)
Chin. Phys. B, 2024, 33 (**12**): 127502. DOI: 10.1088/1674-1056/ad8625

Thickness-dependent magnetic order and phase transition in V_5S_8

Rui-Zi Zhang(张瑞梓), Yu-Yang Zhang(张余洋), Shi-Xuan Du(杜世萱)
Chin. Phys. B, 2020, 29 (**7**): 077504. DOI: 10.1088/1674-1056/ab8db1

Study of magnetic and optical properties of $Zn_{1-x}TM_xTe$ (*TM*=Mn, Fe, Co, Ni) diluted magnetic semiconductors: First principle approach

Q Mahmood, M Hassan, M A Faridi
Chin. Phys. B, 2017, 26 (**2**): 027503. DOI: 10.1088/1674-1056/26/2/027503

SPECIAL TOPIC — Multiferroicity and multicaloric effects

Design of magnetoelectric coupling in ferroelectric metal

Wang Zhang(张旺) and Xue-Zeng Lu(逯学曾)†

Key Laboratory of Quantum Materials and Devices of Ministry of Education, School of Physics, Southeast University, Nanjing 211189, *China*

(Received 15 January 2026; revised manuscript received 7 April 2026; accepted manuscript online 20 April 2026)

Ferroelectricity and metallicity have traditionally been considered difficult to coexist until the experimental discovery of the polar metal $LiOsO_3$ in 2013. Polar metallic materials offer new opportunities for the development of nonvolatile memory. However, simultaneously achieving ferroelectricity, magnetic order, and their strong coupling in a single-phase material remains a challenge. To address this, by using a combination of first-principles calculations and magnetic space group symmetry analysis, we establish a design principle to find magnetoelectric (ME) multiferroics. Our results show that the $(CrSb)_m/(BiSb)_n$ superlattice with altermagnetic CrSb and ferroelectric BiSb can have ferroelectric and magnetic orders and metallicity. Furthermore, the switching of the polarization can effectively control the weak ferromagnetism in the superlattices, in which the strength of this ME coupling is correlated with the magnitude of the induced polarization in the CrSb layers. Our research provides a material design route for exploring multiferroics with ME coupling.

Keywords: magnetoelectric effects and multiferroics, electron density of states, density functional theory calculations

PACS: 75.85.+t, 71.20.–b, 71.15.Mb

DOI: 10.1088/1674-1056/ae6173 **CSTR:** 32038.14.CPB.ae6173

1. Introduction

Ferroelectric metals — a class of materials combining ferroelectric order and metallicity — have attracted much attention in recent years. However, for a long time, it was believed that ferroelectricity and metallicity could not coexist in the same material, primarily because the presence of conduction electrons in metals would screen any internal electric polarization, thereby suppressing ferroelectric behavior. Quantum physics supports this view and demonstrates that nonlocal electrons can give rise to static macroscopic polarization phenomena.[1–3] This long-standing assumption was challenged in 1965, when Anderson and Blount first proposed the concept of a "ferroelectric metal". They theorized that certain martensitic transformations involving the breaking of inversion symmetry could give rise to the emergence of electric polarization.[4] Research was stagnant for nearly four decades until $Cd_2Re_2O_7$ was proposed as a promising candidate.[5] Although it was later characterized as a piezoelectric (i.e., noncentrosymmetric but nonpolar) metal,[6] it revitalized the activities in this field and led to the proposal of many other mechanisms and candidate materials.[7–9] In 2013, a breakthrough was made; Shi *et al.* reported that a similar ferroelectric-like structural phase transition existed in the metal $LiOsO_3$.[10] Their study provided the first experimental evidence confirming the existence of ferroelectric metals, serving as a clear and compelling realization of Anderson and Blount's earlier hypothesis and marking the beginning of a new research direction. In 2014, Xiang revealed the origin of the ferroelectric-like phase transition in metallic $LiOsO_3$ by performing comprehensive DFT calculations and an effective Hamiltonian study. Xiang showed the possible existence of a new class of ferroelectric metal in which the same cation is responsible for both metallicity and ferroelectric-like instability.[11] In the same year, Puggioni and Rondinelli presented a microscopic understanding of a noncentrosymmetric metal (NCSM), leading to a design principle for the theoretical prediction of a polar NCSM transition metal oxide $(Sr,Ca)Ru_2O_6$. Meanwhile, they demonstrated that $(Sr,Ca)Ru_2O_6$ exhibits anisotropic Seebeck coefficients derived from its polar structure.[12]

Subsequently, the field witnessed several important findings. In 2016, Kim *et al.* identified $NdNiO_3$ as another ferroelectric metal, establishing a new pathway for discovering such materials in correlated oxide systems.[13] A major advancement came in 2018, when Fei *et al.* observed switchable out-of-plane electric polarization in bilayer and trilayer WTe_2.[14] Thereafter, Sharma *et al.* discovered that native metallicity and ferroelectricity coexist in bulk crystalline van der Waals WTe_2. They showed that WTe_2 has switchable spontaneous polarization and a natural ferroelectric domain structure at room temperature.[15] These findings represented the experimental demonstration of the coexistence of ferroelectricity and metallicity in a two-dimensional (2D) material, opening the emerging subfield of 2D ferroelectric metals. In the following year, Meng *et al.* reported the first ferroelectric metal that exhibits ferromagnetism.[16] In the same year, Lu *et al.* theoretically demonstrated the existence of ferroelec-

†Corresponding author. E-mail: xuezenglu@seu.edu.cn

© 2026 Chinese Physical Society and IOP Publishing Ltd. All rights, including for text and data mining, AI training, and similar technologies, are reserved.

tricity in ultrathin $LiOsO_3$ films, providing a theoretical basis for the experimental conclusion.[17] In 2020, Marković *et al.* discovered a ferroelectric metallic phase in the Ruddlesden–Popper (RP) oxide $Ca_3Ru_2O_7$, which exhibits a complex interplay among metallicity, polar structure, magnetism, and strong electron correlations.[18] This system has been regarded as a promising platform for studying ME coupling effects. Later, many studies were conducted on $Ca_3Ru_2O_7$.[19–22] For example, Lei *et al.* reported the first experimental observation of polar domain microstructures in $Ca_3Ru_2O_7$.[23] In addition to these landmark studies, several other experimental findings have further enriched the field. All these discoveries underscore the diversity and growing significance of ferroelectric metals in both scientific and technological aspects.

Zhang *et al*. proposed using oxygen polyhedra as fundamental units for modulating material properties.[24] Through atomic-scale manipulation of oxygen vacancy ordering, they successfully synthesized a new functional oxide with a quasi-two-dimensional structure ($Ca_3Co_3O_8$). This material has rich novel properties, such as nonreciprocal resistivity and topological spin textures. However, in this system, modifications in the ferroelectric order still did not induce corresponding changes in magnetic properties, indicating the absence of ME coupling.

So far, the key challenge is how to further explore coupling between ferroelectric order and magnetic properties — along with other novel quantum phenomena — in ferroelectric metallic materials, ultimately enabling the design of nonvolatile information storage devices based on such systems. To address this challenge, Luo *et al*. proposed the concept of 2D hyperferroelectric metals and showed that they can be used to design 2D FM–FE multiferroics.[25] He *et al*. demonstrated a controllable metal–insulator transition, Rashba–Dresselhaus spin splitting effect, and Weyl semimetallic state by applying an electric field in the experimentally available charge-ordered oxide Ag_2BiO_3 using first-principles calculations.[26] In 2026, Zhou *et al*. successfully synthesized a double-layered RP perovskite cobaltate ($Sr_3Co_2O_7$), with intertwined polarity, antiferromagnetism, and metallicity.[27] In our study, we have developed a design principle to achieve strong ME coupling in multiferroics. We have identified that the $(CrSb)_m/(BiSb)_n$ superlattices can have ferroelectric and magnetic orders and metallicity, where m and n denote the number of unit cells of altermagnetic CrSb and ferroelectric BiSb materials, respectively. Our results further demonstrate that within these superlattices, polarization switching can effectively modulate weak ferromagnetic behavior. Moreover, the strength of polarization is positively correlated with the extent of modulation in wFM: the stronger the polarization, the more pronounced the magnetic changes induced by polarization reversal.

2. Methods

We performed our first-principles calculations using density functional theory (DFT), as implemented in the Vienna *Ab initio* Simulation Package (VASP).[28,29] The electron–ion interactions were modeled with the projector augmented wave (PAW) method,[30] and the Perdew–Burke–Ernzerhof (PBE) functional[31] was used for the exchange–correlation interaction. To describe the strong electron correlations in the Cr 3d orbitals, the DFT plus Hubbard U approach was used with the simplified rotationally invariant method.[32] An effective on-site Coulomb parameter $U = 0.25$ eV[33] was applied exclusively to Cr atoms. A plane-wave kinetic energy cutoff of 400 eV was adopted. The geometry optimization and static self-consistent calculations used a gamma-centered k-point mesh of $5 \times 5 \times 1$ for all the superlattices. In our calculations, the force and electronic self-consistent convergence was achieved when the energy differences were less than 1×10^{-6} eV and the force components were smaller than 0.01 eV/Å. The polarization was computed by adopting a point charge model because of the invalid application of the Born effective charge model or Berry phase method to polar metals, in which the changes in the ionic displacements between the up-polarized and down-polarized states are multiplied by the nominal valence charges of the ions.[34]

3. Results and discussion

We begin by elucidating the design principles for realizing ME coupling. As illustrated in Fig. 1(a), our theory imposes the following two essential requirements on the space-group symmetry of magnetic materials. (1) The magnetic atoms occupied by spin-up and spin-down states must not be related by translational symmetry. (2) Any symmetries between the antiferromagnetic (AFM) sublattices must be broken under an external electric field. Our theoretical framework does not require the inclusion of spin–orbit coupling (SOC); instead, the emergence of weak magnetism in the system originates from symmetry breaking between spin-up and spin-down sublattices.

To make the ME coupling nonvolatile, we need to construct a structure combining ferroelectric materials with AFM materials, instead of using an electric field, to break the symmetry between the antiparallel spins. Here, we choose the ferroelectric material BiSb and the altermagnetic material CrSb to elucidate our design principle. BiSb is a conventional ferroelectric material with $R3m$ symmetry,[35,36] whereas the CrSb ground-state structure has $P63/mmc$ symmetry.[33,37,38] The altermagnetic CrSb naturally meets criterion 1, as there is no translational symmetry between the antiparallel spins. The altermagnetic feature of CrSb, that is, nonrelativistic spin splitting in the band structure, has been demonstrated

in previous studies[33,37–41] and was also computed in our study (supplementary Fig. S1). This feature is distinct from that of conventional AFM materials because of their spin-opposite sublattices linked by real-space rotation or mirror symmetries,[33,37,38,40,41] such as $\{C2|\ 2_{001}|\ 0\ 0\ 1/2\}$, $\{C2|\ 6^{-}_{001}\ |\ 0\ 0\ 1/2\}$, $\{C2|\ 6^{+}_{001}\ |\ 0\ 0\ 1/2\}$, $\{C2|\ 2_{1-10}\ |\ 0\ 0\ 1/2\}$, $\{C2|\ 2_{120}\ |\ 0\ 0\ 1/2\}$, $\{C2|\ 2_{210}\ |\ 0\ 0\ 1/2\}$, $\{m_{001}\ |\ 0\ 0\ 1/2\}$, $\{C2|\ -6^{-}_{001}\ |\ 0\ 0\ 1/2\}$, $\{C2|-6^{+}_{001}\ |\ 0\ 0\ 1/2\}$, $\{C2|m_{1-10}\ |\ 0\ 0\ 1/2\}$, $\{C2|m_{120}\ |\ 0\ 0\ 1/2\}$, and $\{C2|m_{210}\ |\ 0\ 0\ 1/2\}$ in bulk CrSb. These characteristics lead to spin splitting in the band structure even in the absence of SOC effects.[42–47]

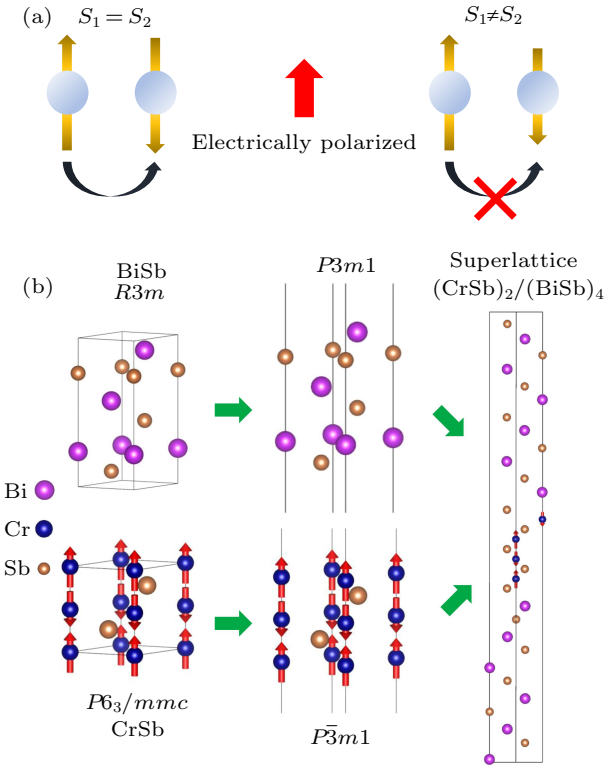


Fig. 1. (a) Illustration of symmetry breaking between the magnetic atoms occupied by antiparallel spins by applying an electric field. (b) Superlattice structure composed of ferroelectric material BiSb and altermagnetic material CrSb. Red arrows indicate the spin directions of the Cr atoms.

When combining CrSb and BiSb in a superlattice, we find that the symmetries of CrSb and BiSb in their slab structures are both reduced to $P3m1$ without structural relaxation. After relaxation of the in-plane lattices and atomic positions, the slab structures of CrSb and BiSb adopt the $P\bar{3}m1$ and $P3m1$ symmetries, respectively. In $P\bar{3}m1$, the symmetries connecting the antiparallel spins are $\{C2|2_{110}\ |0\}$, $\{C2|2_{100}\ |0\}$, $\{C2|2_{010}\ |0\ \}$, $\{C2|-1|0\}$, $\{C2|-3^{+}_{001}\ |0\}$, and $\{C2|-3^{-}_{001}\ |0\}$. Thus, altermagnetic spin ordering is absent in the $P\bar{3}m1$ structure of CrSb because of the existence of $\{C2|-1|0\}$. However, application of an electric field along the [001] direction (Fig. 1(a)) can break all the symmetries between the antiparallel spins in $P\bar{3}m1$, thereby satisfying the second criterion as mentioned above. Consequently, in the CrSb/BiSb superlattice, the polarization of BiSb should induce a net wFM in the CrSb component.

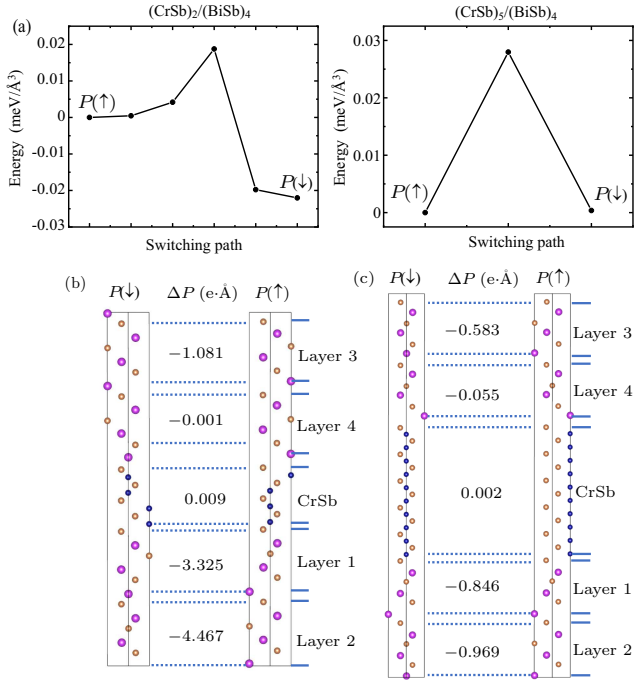


Fig. 2. (a) Computed energy barrier between $P(\uparrow)$ and $P(\downarrow)$ for the $(CrSb)_2/(BiSb)_4$ and $(CrSb)_5/(BiSb)_4$ superlattices. (b) Structures with opposite polarizations of $(CrSb)_2/(BiSb)_4$. (c) Structures with opposite polarizations of $(CrSb)_5/(BiSb)_4$.

Table 1. Changes in polarization between states with opposite polarizations of the investigated superlattices.

Superlattice	$\lvert\Delta P_X\rvert$ (μC/cm^2)	$\lvert\Delta P_Y\rvert$ (μC/cm^2)	$\lvert\Delta P_Z\rvert$ (μC/cm^2)	$\lvert\Delta P_{tot}\rvert$ (μC/cm^2)	$\lvert\Delta P_Z\rvert$ per CrSb layer (e·Å)
$(CrSb)_1/(BiSb)_4$	0.038	0.057	0.278	0.286	0.0003
$(CrSb)_2/(BiSb)_4$	0.169	0.245	16.159	16.161	0.0045
$(CrSb)_5/(BiSb)_4$	1.386	0.156	8.435	8.549	0.0004

Next, we performed first-principles calculations on these superlattice systems to determine their ground-state structures. The results show that the relaxation of the CrSb/BiSb superlattice with the initial $P\bar{3}m1$ and $P3m1$ symmetries in the CrSb and BiSb components, respectively, led to Cm structures for our studied superlattice periods, i.e., $(CrSb)_1/(BiSb)_4$, $(CrSb)_2/(BiSb)_4$, and $(CrSb)_5/(BiSb)_4$. Furthermore, in our climbing nudged elastic band (NEB) calculations, two stable polar states with Cm symmetries were demonstrated, as shown in Fig. 2 for $(CrSb)_2/(BiSb)_4$ and $(CrSb)_5/(BiSb)_4$. The computed changes in polarization between the bipolar states ranged from 8.549 μC/cm^2 to 16.161 μC/cm^2 by varying the period of the CrSb component (Table 1). In addition, the switching barrier in the superlattices was smaller than that in the bulk BiSb, which had a barrier of 2.079 meV/Å^3 (supplementary Fig. S2). The asymmetric bipolar states in

$(CrSb)_2/(BiSb)_4$ can be attributed to the asymmetric magnetic states arising from symmetry breaking among the antiparallel spins, as discussed below. The energy differences became negligible in $(CrSb)_5/(BiSb)_4$ because the magnetic states between the bipolar states were not changed as much as those in $(CrSb)_2/(BiSb)_4$.

Figure 3 presents the density of states (DOS) for $(CrSb)_2/(BiSb)_4$ and $(CrSb)_5/(BiSb)_4$, revealing that both superlattices exhibit metallic behavior originating primarily from the Bi-p, Sb-p, and Cr-d orbitals. These systems can therefore be classified as polar metals, in which polar order and metallicity coexist in a single phase. Although switchable polar order in a metal phase, which is referred to as a ferroelectric metal, has rarely been reported, tip-pressure-induced strain gradients and femtosecond techniques can be used to control the polar order, thereby realizing magnetoelectric coupling in polar metals.[24] As shown in Fig. 4, the layer-resolved DOS indicates that the BiSb components adopted a polar character, in contrast to their bulk semiconductor form. Moreover, one side of the BiSb component exhibited a higher electron concentration at the Fermi level than the other. This resulted in an asymmetric variation in the layer-resolved polarization of BiSb, which increased with greater electron concentration at the Fermi level. Such an asymmetric polarization change may further stabilize the polar state in the metallic CrSb/BiSb superlattices, suggesting that metallicity helps sustain the polar ground state within the BiSb layers. Thus, two main effects contribute to the asymmetric layer-resolved polarization: (1) metallicity promotes the stabilization of the polar mode, and (2) the interface with centrosymmetric CrSb reduces the polar displacement. Finally, a modest polarization was also observed in the CrSb layers. Although small, this polarization played a critical role in breaking symmetry between antiparallel spins, ultimately leading to a net weak ferromagnetic order even in the absence of spin–orbit coupling. These findings are consistent with our earlier symmetry analysis. In the magnetic calculations, a Néel spin ordering was adopted as in bulk CrSb. Because of the symmetry breaking between the AFM sublattices, there was wFM (Table 1). This induced wFM was proportional to the changes in polarization in the CrSb layers between the bipolar states. For example, $(CrSb)_2/(BiSb)_4$ exhibited the largest polarization changes, thus leading to the largest change in wFM in the CrSb layers between the bipolar states (Table 2 and Figs. 2(b) and 2(c)). The $(CrSb)_1/(BiSb)_4$ and $(CrSb)_5/(BiSb)_4$ superlattices had similar polar displacements in the CrSb layers, but the induced wFM distribution in the $(CrSb)_5/(BiSb)_4$ superlattice was more symmetric than that in the $(CrSb)_1/(BiSb)_4$ superlattice. This led to a different total wFM in the CrSb layers between the two superlattices, despite their similar polar displacements. Thus, a thicker CrSb layer may require a larger polar displacement to induce an asymmetric change in wFM compared to a thinner CrSb layer (Fig. 5).

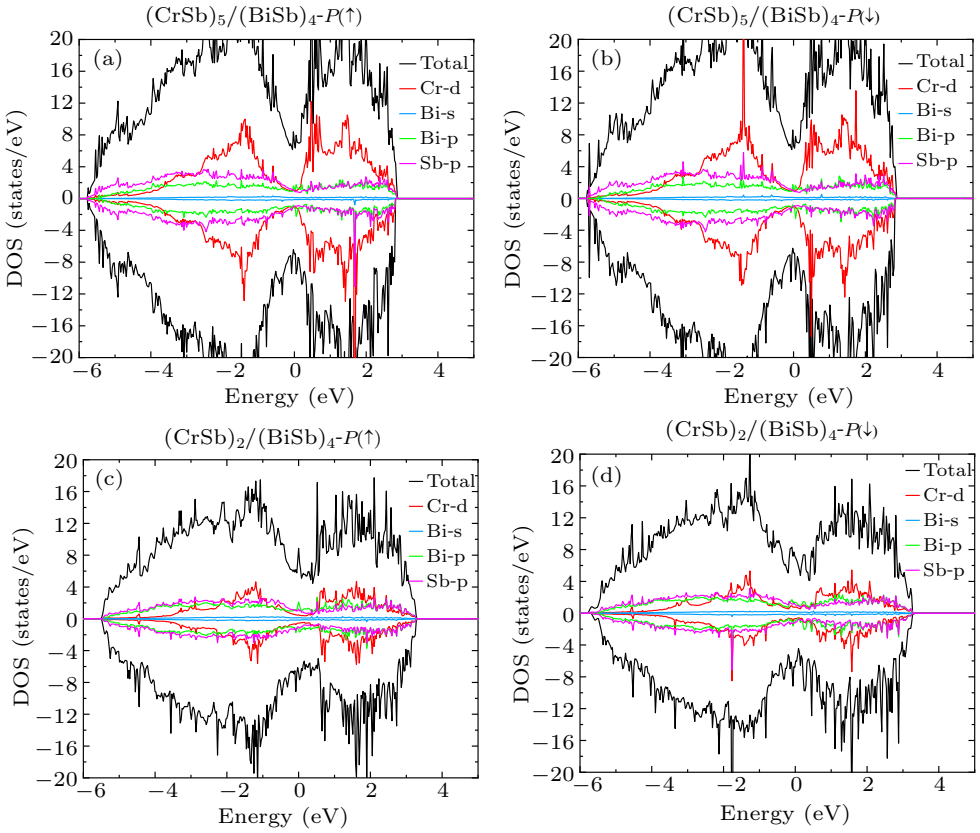


Fig. 3. (a) Computed DOS for $(CrSb)_5/(BiSb)_4$-$P(\uparrow)$ and $(CrSb)_5/(BiSb)_4$-$P(\downarrow)$. (b) Computed DOS for $(CrSb)_2/(BiSb)_4$-$P(\uparrow)$ and $(CrSb)_2/(BiSb)_4$-$P(\downarrow)$.

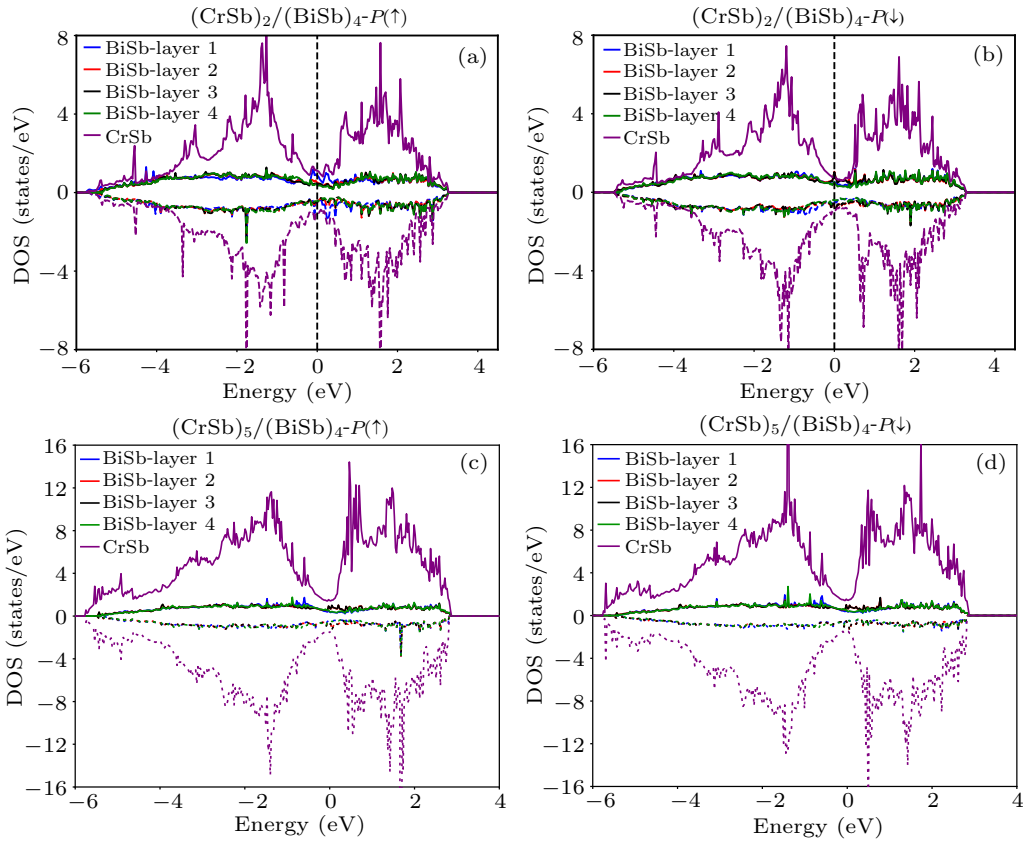


Fig. 4. Layer-resolved DOS for down-polar and up-polar states of the 2:4 and 5:4 superlattices. The CrSb and BiSb layers are shown in Fig. 2.

Table 2. Changes in wFM along the principal AFM vector in the studied superlattices when changing the polarization, with projections of the magnetization onto the s, p, and d orbitals and the total magnetization.

Superlattice	ΔM_s (μ_B/Cr)	ΔM_p (μ_B/Cr)	ΔM_d (μ_B/Cr)	ΔM_{tot} (μ_B/Cr)
$(CrSb)_1/(BiSb)_4$	0	–0.0005	–0.0025	–0.003
$(CrSb)_2/(BiSb)_4$	0.00173	–0.02161	–0.00884	–0.02872
$(CrSb)_5/(BiSb)_4$	–0.00007	–0.00038	–0.00042	–0.00087

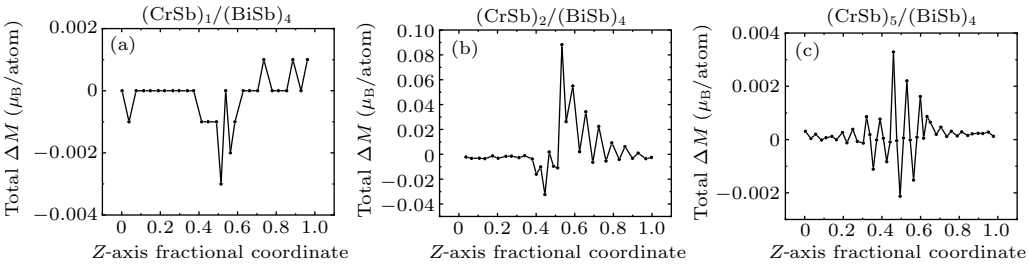


Fig. 5. Changes in induced wFM as a function of layer position along the z direction in the 1:4, 2:4, and 5:4 superlattices between the $P(\downarrow)$ and $P(\uparrow)$ states.

Table 3. Computed directions of MA and energy differences ΔE between spin orderings along the [001] direction and the in-plane easy axis.

Superlattice	MA direction	ΔE (meV/Å^3)
$(CrSb)_1/(BiSb)_4$-$P(\uparrow)$	0 0 1	–0.00101
$(CrSb)_1/(BiSb)_4$-$P(\downarrow)$	0 0 1	–0.00103
$(CrSb)_2/(BiSb)_4$-$P(\uparrow)$	0 0 1	–0.00579
$(CrSb)_2/(BiSb)_4$-$P(\downarrow)$	0 0 1	–0.00454
$(CrSb)_5/(BiSb)_4$-$P(\uparrow)$	0 0 1	–0.00170
$(CrSb)_5/(BiSb)_4$-$P(\downarrow)$	0 0 1	–0.00164

By considering SOC effects in the structural relaxation and magnetic calculations of the $(CrSb)_2/(BiSb)_4$ superlattice, the changes in wFM due to a change in polarization are reduced. For example, wFM is 0.029 μ_B/Cr without SOC effects and decreases to 0.005 μ_B/Cr when SOC effects are included. The DFT+U+SOC calculations further showed that the computed magnetic anisotropy (MA) of all the studied superlattices lies along the [001] direction (Table 3). The magnetic space group symmetry is Cm', in which the mirror symmetry connects only parallel spins. Because the energy differences between the [001] and in-plane easy-axis directions are very small, a spin-flop induced by a magnetic field along [001] may tune the MA to be in-plane. When the MA is in-plane, a tunable nonreciprocal resistance may arise by changing the polar

states, where the nonreciprocal resistance is proportional to $\sim(\boldsymbol{P}\times\boldsymbol{M})$, where $\boldsymbol{P}$ and $\boldsymbol{M}$ represent polarization and magnetization, respectively.[24] This occurs because a change in polarization simultaneously changes the magnitude of $\boldsymbol{M}$, resulting in a change in nonreciprocal resistance as $\sim(\boldsymbol{P}\times\boldsymbol{M})$. Thus, a tunable nonreciprocal resistance driven by polarization may be realized in $(CrSb)_2/(BiSb)_4$, which exhibits both large polarization and sizable $\Delta\boldsymbol{M}$.

4. Conclusions

We have demonstrated a deterministic approach to achieving strong ME coupling in a series of metallic multiferroic superlattices. The design principle leverages symmetry breaking between the AFM sublattices of the altermagnetic CrSb exerted by the conventional ferroelectric BiSb. Our key findings are as follows: (1) the designed $(CrSb)_m/(BiSb)_n$ superlattices exhibit bistable polar states with metallicity; and (2) most importantly, the switching of the polarization effectively modulates wFM in the superlattices, with the strength of this ME coupling increasing as the polarization magnitude grows through variation of the CrSb components. These results further confirm that the ME coupling in the superlattices is attributable to the symmetry breaking induced by the ferroelectric BiSb component, which does not rely on SOC. Our symmetry-breaking mechanism for designing ME multiferroics may open a new avenue for discovering high-performance ME materials by deliberately combining altermagnets with ferroelectrics.

Acknowledgements

W.Z. and X.-Z.L. were supported by the National Natural Science Foundation of China (Grant No. 12474081), the Open Research Fund of the Key Laboratory of Quantum Materials and Devices at Southeast University (Ministry of Education), and the Start-up Research Fund of Southeast University. The DFT calculations were performed on high-performance computers supported by the Big Data Computing Center of Southeast University.

References

[1] Resta R 2002 *J. Phys. Condens. Matter* **14** R625
[2] Bhowal S and Spaldin N A 2023 *Annu. Rev. Mater. Res.* **53** 53
[3] Cohen-Tannoudji C, Dupont-Roc J and Grynberg G 1997 *Photons and atoms: introduction to quantum electrodynamics* (John Wiley & Sons) p. 292
[4] Anderson P W and Blount E I 1965 *Phys. Rev. Lett.* **14** 217
[5] Sergienko I A, Keppens V, McGuire M, *et al*. 2004 *Phys. Rev. Lett.* **92** 065501
[6] Ishibashi Y and Iwata M 2010 *J. Phys. Soc. Jpn.* **79** 044604
[7] Filippetti A, Fiorentini V, Ricci F, *et al*. 2016 *Nat. Commun.* **7** 11211
[8] Kolodiazhnyi T, Tachibana M, Kawaji H, *et al*. 2010 *Phys. Rev. Lett.* **104** 147602
[9] Urru A, Ricci F, Filippetti A, *et al*. 2020 *Nat. Commun.* **11** 4922
[10] Shi Y, Guo Y, Wang X, *et al*. 2013 *Nat. Mater.* **12** 1024
[11] Xiang H J 2014 *Phys. Rev. B* **90** 094108
[12] Puggioni D and Rondinelli J M 2014 *Nat. Commun.* **5** 3432
[13] Kim T H, Puggioni D, Yuan Y, *et al*. 2016 *Nature* **533** 68
[14] Fei Z, Zhao W, Palomaki T A, *et al*. 2018 *Nature* **560** 336
[15] Sharma P, Xiang F X, Shao D F, *et al*. 2019 *Sci. Adv.* **5** eaax5080
[16] Meng M, Wang Z, Fathima A, *et al*. 2019 *Nat. Commun.* **10** 5248
[17] Lu J, Chen G, Luo W, *et al*. 2019 *Phys. Rev. Lett.* **122** 227601
[18] Marković I, Watson M D, Clark O J, *et al*. 2020 *Proc. Natl. Acad. Sci. USA* **117** 15524
[19] Stone G, Puggioni D, Lei S, *et al*. 2019 *Phys. Rev. B* **99** 014105
[20] Kikugawa N, Sokolov D A, Sow C, *et al*. 2021 *J. Phys. Soc. Jpn.* **90** 103704
[21] Lamura G, Das D, Shang T, *et al*. 2022 *J. Magn. Magn. Mater.* **551** 169138
[22] Puggioni D, Horio M, Chang J, *et al*. 2020 *Phys. Rev. Res.* **2** 023141
[23] Lei S, Gu M, Puggioni D, *et al*. 2018 *Nano Lett.* **18** 3088
[24] Zhang J, Shen S, Puggioni D, *et al*. 2024 *Nat. Mater.* **23** 912
[25] Luo W, Xu K and Xiang H 2017 *Phys. Rev. B* **96** 235415
[26] He J, Di Sante D, Li R, *et al*. 2018 *Nat. Commun.* **9** 492
[27] Zhou Y, Shu X, Zhang Y, *et al*. 2026 *Nat. Mater.* **25** 231
[28] Kresse G and Furthmüller J 1996 *Phys. Rev. B* **54** 11169
[29] Kresse G and Joubert D 1999 *Phys. Rev. B* **59** 1758
[30] Blöchl P E 1994 *Phys. Rev. B* **50** 17953
[31] Perdew J P, Burke K and Ernzerhof M 1996 *Phys. Rev. Lett.* **77** 3865
[32] Dudarev S L, Botton G A, Savrasov S Y, *et al*. 1998 *Phys. Rev. B* **57** 1505
[33] Park I J, Kwon S and Lake R K 2020 *Phys. Rev. B* **102** 224426
[34] Kumagai Y and Spaldin N A 2013 *Nat. Commun.* **4** 1540
[35] Liu H, Wang J, Han Y, *et al*. 2022 *J. Mater. Chem. C* **10** 3531
[36] Singh S and Romero A H 2017 *Phys. Rev. B* **95** 165444
[37] Reimers S, Odenbreit L, Šmejkal L, *et al*. 2024 *Nat. Commun.* **15** 2116
[38] Zeng M, Zhu M Y, Zhu Y P, *et al*. 2024 *Adv. Sci.* **11** 2406529
[39] Ito T, Ido H and Motizuki K 2007 *J. Magn. Magn. Mater.* **310** e558
[40] Ding J, Jiang Z, Chen X, *et al*. 2024 *Phys. Rev. Lett.* **133** 206401
[41] Yang G, Li Z, Yang S, *et al*. 2025 *Nat. Commun.* **16** 1442
[42] Cheong S W and Huang F T 2024 *Npj Quantum Mater.* **9** 13
[43] Bai L, Feng W, Liu S, *et al*. 2024 *Adv. Funct. Mater.* **34** 2409327
[44] Šmejkal L, Sinova J and Jungwirth T 2022 *Phys. Rev. X* **12** 031042
[45] Zhang H M, Ji C A, Zhu T, *et al*. 2025 *Phys. Rev. Lett.* **135** 176701
[46] Mazin I 2022 *Phys. Rev. X* **12** 040002
[47] Šmejkal L, Sinova J and Jungwirth T 2022 *Phys. Rev. X* **12** 040501